OPEN

Aggregation tendency of guest Fe in $NaCo_{1-x}Fe_xO_2$ ($x < 0.1$) as investigated by systematic EXAFS analysis

Toshiaki Moriya[1], Hideharu Niwa[1,2,3]✉, Hiroaki Nitani[4] & Yutaka Moritomo[1,2,3]✉

In transition metal (M) compounds, the partial substitution of the host transition metal (M_h) to guest one (M_g) is effective to improve the functionality. To microscopically comprehend the substitution effect, degree of distribution of M_g is crucial. Here, we propose that a systematic EXAFS analysis against the M_g concentration can reveal the spatial distribution of M_g. We chose $NaCo_{1-x}Fe_xO_2$ as a prototypical M compound and investigated the local intermetal distance around the guest Fe $[d_{Fe-M}(x)]$ against Fe concentration (x). $d_{Fe-M}(x)$ steeply increased with x, reflecting the larger ionic radius of high-spin Fe^{3+}. The x-dependence of $d_{Fe-M}(x)$ was analyzed by an empirical equation, $d_{Fe-M}(x) = sxd_{Fe-Fe} + (1 - sx)d_{Fe-Co}$, where d_{Fe-Fe} and d_{Fe-Co} are the Fe–Fe and Co–Fe distances, respectively. The parameter s represents degree of distribution of Fe; $s = 1, > 1, < 1$ are for random, attractive, and repulsive distribution, respectively. The obtained s value (= 4.8) indicates aggregation tendency of guest Fe.

The partial substitution of the host transition metal (M_h) to the guest transition metal (M_g) is an effective method to improve the functionality of the materials, such as its electrochemical[1–6], magnetic[7–9], and dielectric[10] properties. For example, $NaFe_{0.5}Co_{0.5}O_2$[1] with an O3-type layered structure shows a high discharge capacity of 160 mAh/g and good cyclability, which is much higher than those of the parent $O3$-$NaFeO_2$ and $O3$-$NaCoO_2$. To microscopically comprehend the substitution effect, degree of distribution (random, attractive, and repulsive distribution: Fig. 1) of M_g is a crucial parameter. In the random distribution (Fig. 1a), the probability to find M_g at the nearest-neighboring site of M_g is the same as the mixing ratio (x) of M_g. The probability is higher than x in the attractive distribution (Fig. 1b) while it is lower than x in the repulsive distribution (Fig. 1c). Thus, we can describe the degree of distribution with parameter s that modifies the probability to find M_g at the nearest-neighboring site as sx. $s = 1, > 1, < 1$ represent the random, attractive, and repulsive distribution, respectively. Here, we propose that a systematic extended X-ray absorption fine structure (EXAFS) analysis against the M_g concentration can reveal the spatial distribution of M_g. The K-edge EXAFS analysis of $3d$ transition metals (Ms) is a powerful technique to determine the local intermetal distance around the corresponding M in the mixed compounds. Importantly, the observed intermetal distance $[d_{Mg-M}(x)]$ around M_g is the probability-weighted average of d_{Mg-Mg} and d_{Mg-Mh}, because a difference between d_{Mg-Mg} and d_{Mg-Mh} is too small to separate. Then, we can extract the parameter s from systematic $d_{Mg-M}(x)$ data against x.

The O3-type layered transition metal oxides, $O3$-$NaMO_2$ (M = Cr, Fe, and Co), show quite simple crystal structure with alternating MO_2 layers and Na sheets[11]. The MO_2 layer consists of edge-sharing MO_6 octahedra formed by covalent bonding. Especially, $O3$-$NaFeO_2$ and $O3$-$NaCoO_2$ form solid solution in the entire composition range. $O3$-$NaFeO_2$ has been investigated due to its electrochemical[12], magnetic[13,14] properties. On the other hand, $O3$-$NaCoO_2$ has been investigated due to its electrochemical[15], thermoelectric[16], and superconductive[17] properties. In addition, the ionic radius (r = 0.645 Å) of high-spin Fe^{3+} is much larger than that (r = 0.545 Å) of low-spin Co^{3+}. In this sense, $O3$-$NaCo_{1-x}Fe_xO_2$ is a suitable system for investigation of degree of distribution of Fe.

¹Graduate School of Pure and Applied Sciences, University of Tsukuba, Tsukuba 305-8571, Japan. ²Faculty of Pure and Applied Sciences, University of Tsukuba, Tsukuba 305-8571, Japan. ³Tsukuba Research Center for Energy Materials Science (TREMS), University of Tsukuba, Tsukuba 305-8571, Japan. ⁴Institute of Materials Science, High Energy Accelerator Research Organization (KEK), Tsukuba 305-0801, Japan. ✉email: niwa.hideharu.ga@u.tsukuba.ac.jp; moritomo.yutaka.gf@u.tsukuba.ac.jp
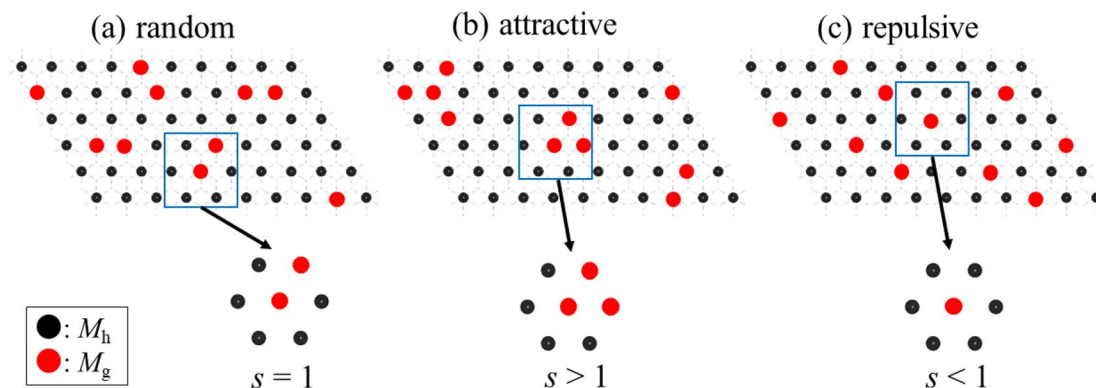
Figure 1. Distribution of the partial substituted element (M_g): (**a**) random, (**b**) attractive, and (**c**) repulsive distribution. In the present case, the mixing ratio x is 1/6. So, the probability to find M_g at the nearest-neighboring site is 1/6 in (**a**) random distribution, while it is higher (lower) than 1/6 in the (**b**) attractive [(**c**) repulsive] distribution.
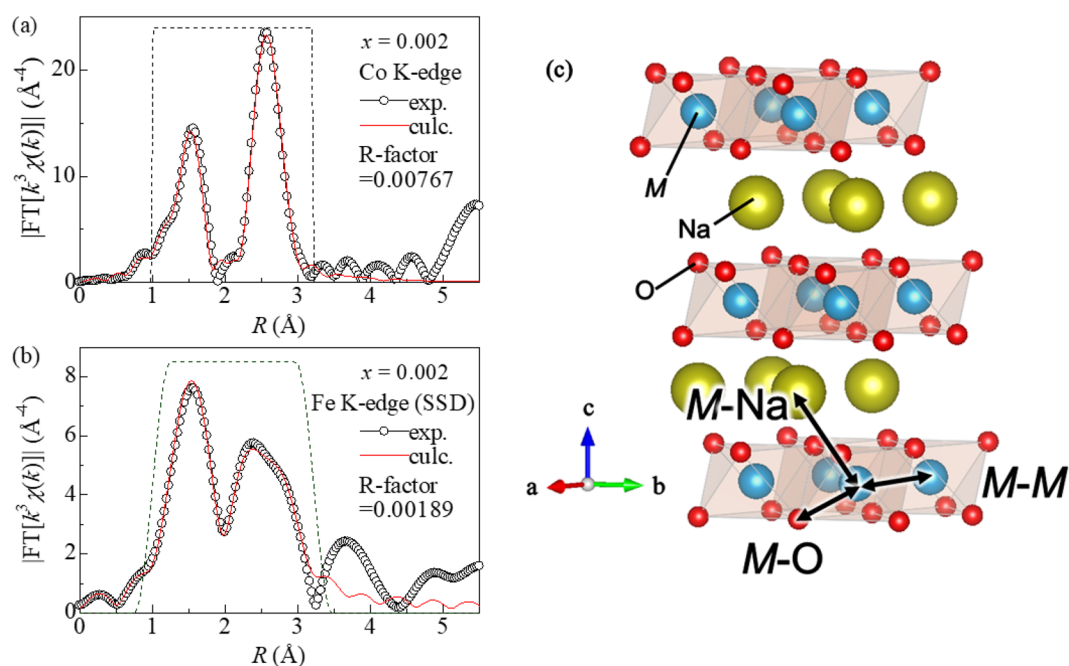

Figure 2. Fourier transforms of k^3-weighted (**a**) Co and (**b**) Fe K-edge EXAFS spectra for $NaCo_{0.998}Fe_{0.002}$ without phase shift correction. Red curves are the results of the least-squares curve-fitting with the EXAFS equation in the R range from 1.0 to 3.22 Å. (**c**) Schematic structure of O3-NaMO_2. The first- (M–O), the second-(M–M), and the third (M–Na) scattering paths are indicated by allows.

We chose $NaCo_{1-x}Fe_xO_2$ as a prototypical transition metal compound and systematically investigated the local intermetal distance around the host Co [$d_{Co-M}(x)$] and the guest Fe [$d_{Fe-M}(x)$] against x. The x-dependence of $d_{Fe-M}(x)$ was analyzed by an empirical equation, $d_{Fe-M}(x) = sxd_{Fe-Fe} + (1 - sx)d_{Fe-Co}$, where d_{Fe-Fe} and d_{Fe-Co} are the Fe–Fe and Co–Fe distances, respectively. The obtained s value (= 4.8) indicates aggregation tendency of guest Fe in $NaCo_{1-x}Fe_xO_2$.

Results

Local structure around transition metal. Figure 2a,b show prototypical Fourier transformation of the $\chi(k)k^3$–R plots around the host Co and the guest Fe in $NaCo_{0.998}Fe_{0.002}O_2$, respectively. χ and k are the oscillatory components of the normalized absorption and wavenumber, respectively. In the Co K-edge EXAFS spectra (Fig. 2a), two intense peaks are observed at around 1.5 Å and 2.4 Å (without phase shift correction), which are assigned to the paths to the first- (O) and second- (M) nearest neighbor elements, respectively (Fig. 2c). The corresponding peaks are observed in the Fe K-edge EXAFS spectra (Fig. 2b). With including contributions from first-(O), second-(M), and third-(Na) nearest neighbor elements, we performed least-squares fittings with the EXAFS equation in the R range from 1.0 to 3.22 Å. Thus, obtained parameters around Co and Fe are listed in

x	d_{Co-O} (Å)	σ^2_{Co-O} (Å^2)	d_{Co-M} (Å)	σ^2_{Co-M} (Å^2)	d_{Co-Na} (Å)	σ^2_{Co-Na} (Å^2)
0.000	1.918 (11)	0.004 (1)	2.875 (9)	0.004 (1)	3.092 (10)	0.002 (2)
0.002	1.914 (10)	0.004 (1)	2.869 (8)	0.004 (1)	3.095 (10)	0.002 (1)
0.006	1.917 (10)	0.004 (1)	2.877 (8)	0.004 (1)	3.089 (9)	0.003 (2)
0.012	1.912 (7)	0.004 (1)	2.867 (6)	0.004 (1)	3.086 (8)	0.004 (1)
0.024	1.917 (9)	0.004 (1)	2.872 (6)	0.004 (1)	3.081 (10)	0.005 (2)
0.060	1.918 (6)	0.004 (1)	2.875 (5)	0.004 (1)	3.081 (8)	0.005 (2)

Table 1. Structural parameters of $NaCo_{1-x}Fe_xO_2$ obtained by Co K-edge EXAFS analyses. The spectra were recorded in transmission mode. d_{Co-O} and d_{Co-M} are Co–O and Co–M distances, respectively. σ^2_{Co-O} and σ^2_{Co-M} are the Debye–Waller factor for each shell. Uncertainty of the last digit(s) is given in parentheses.

x	d_{Fe-O} (Å)	σ^2_{Fe-O} (Å^2)	d_{Fe-M} (Å)	σ^2_{Fe-M} (Å^2)	d_{Fe-Na} (Å)	σ^2_{Fe-Na} (Å^2)
0.002	2.003 (13)	0.005 (1)	2.916 (9)	0.006 (1)	3.116 (26)	0.013 (7)
0.006	1.995 (10)	0.007 (1)	2.915 (6)	0.007 (1)	3.120 (16)	0.012 (5)
0.012 (F)	1.995 (15)	0.009 (2)	2.910 (11)	0.008 (2)	3.100 (21)	0.009 (5)
0.012 (T)	2.003 (18)	0.005 (1)	2.919 (9)	0.004 (1)	3.169 (28)	0.011 (12)
0.024	2.004 (12)	0.003 (1)	2.923 (7)	0.005 (1)	3.160 (24)	0.013 (9)
0.060	2.014 (8)	0.003 (1)	2.947 (5)	0.006 (1)	3.153 (18)	0.016 (5)

Table 2. Structural parameters of $NaCo_{1-x}Fe_xO_2$ obtained by Fe K-edge EXAFS analyses. The spectra were recorded in fluorescence ($x = 0.002$, 0.006, and 0.012 (F)) or transmission ($x = 0.012$ (T), 0.024, and 0.060) modes. d_{Fe-O} and d_{Fe-M} are Fe–O and Fe–M distances, respectively. σ^2_{Fe-O} and σ^2_{Fe-M} are the Debye–Waller factor for each shell. Uncertainty of the last digit(s) is given in parentheses.

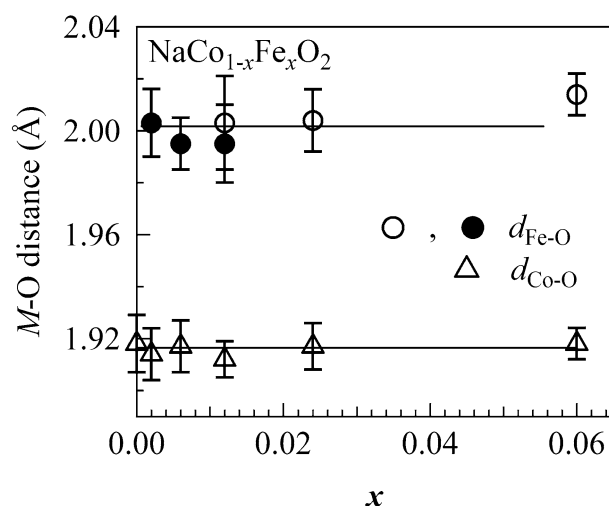**Figure 3.** Co–O (d_{Co-O}) and Fe–O (d_{Fe-O}) distance of $NaCo_{1-x}Fe_xO_2$ against x. Straight lines are guides for the eye. Open and closed symbols represent the corresponding EXAFS data obtained in the transmission and fluorescence modes, respectively.

Tables 1 and 2, respectively. The Co–O distance [$d_{Co-O} = 1.918(11)$ Å] and Co–Co distance [$d_{Co-Co} = 2.875(9)$ Å] in $NaCoO_2$ are close to the crystallographic values, 1.935 Å and 2.890 Å[18], within experimental error.

Co and Fe K-edge X-ray absorption near edge structure (XANES) spectra for $NaCo_{1-x}Fe_xO_2$ are shown in Figs. S1 and S2 in the supplementary information, respectively. We observed no detectable peak-shift in Co K-edge XANES spectra. We observed no detectable main peak shift for Fe K-edge XANES spectra, even though the spectral shape is slightly distorted due to the self-absorption effect[19]. These observations indicate that electronic states of the host Co and guest Fe are almost the same.

Interatomic distances (d_{Co-O} and d_{Fe-O}) to the nearest-neighboring oxygen. Figure 3 shows the Co–O (d_{Co-O}) and the Fe–O (d_{Fe-O}) distances in $NaCo_{1-x}Fe_xO_2$ against x. As indicated by the eye-guide straight lines, d_{Co-O} and d_{Fe-O} are almost constant against x within experimental error. The larger error bars in d_{Fe-O} are originated in the lower concentration of Fe and the resultant worse S/N ratio of the EXAFS signal. The robust

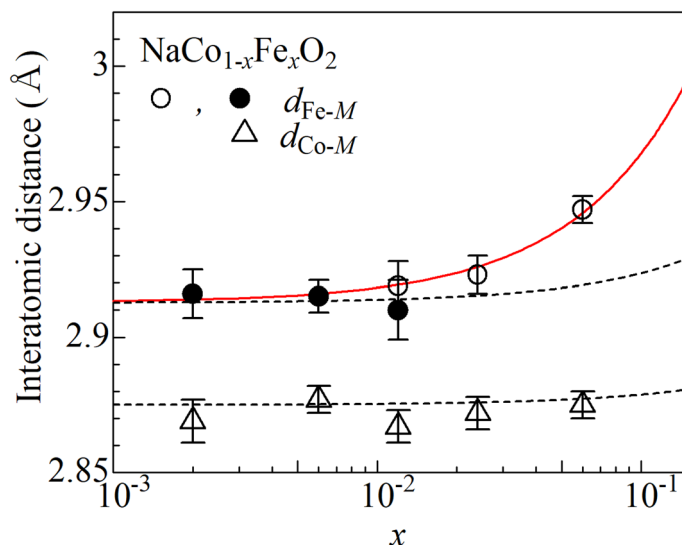**Figure 4.** Co–M (d_{Co-M}) and Fe–M (d_{Fe-M}) distances of NaCo$_{1-x}$Fe$_x$O$_2$ against x. Open and closed symbols represent the corresponding EXAFS data obtained in the transmission and fluorescence modes, respectively. Broken curves are calculated by $d_{Co-M}(x) = xd_{Co-Fe} + (1-x)d_{Co-Co}$ and $d_{Fe-M}(x) = xd_{Fe-Fe} + (1-x)d_{Fe-Co}$, respectively. Red solid curve is the least-square fitting by the empirical equation; $d_{Fe-M}(x) = sxd_{Fe-Fe} + (1-sx)d_{Fe-Co}$ ($s = 4.8$).

nature of d_{Co-O} and d_{Fe-O} is ascribed to the fact that the Co (Fe) sites are surrounded by six oxygens as MO_6 even in the mixed crystal. A similar robust nature of the interatomic distance to the first nearest elements is reported in the mixed crystal of metal-hexacyanides[20], in which M is surrounded by six cyanide as M(NC)$_6$.

Interatomic distances (d$_{Co-M}$ and d$_{Fe-M}$) to the nearest-neighboring transition metals. Figure 4 shows the Fe–M (d_{Fe-M}) and Co–M (d_{Co-M}) distances in NaCo$_{1-x}$Fe$_x$O$_2$ against x. d_{Co-O} is apparently robust against x. This is partly because difference between d_{Co-Co} [= 2.875(9) Å] and d_{Co-Fe} [= 2.91; extrapolated value of $d_{Fe-M}(x)$ at $x = 0$] is too small to detect x-dependence of $d_{Co-M}(x)$. Looking at Fig. 4, one may notice that $d_{Fe-M}(x)$ shows significant x-dependence and increases with x, reflecting larger ionic radius of high-spin Fe^{3+} than that of low-spin Co^{3+}.

First, let us consider the situation of random distribution of the guest Fe. As explained in the introduction section, $d_{Co-M}(x)$ [$d_{Fe-M}(x)$] determined by the EXAFS analyses corresponds to the probability-weighted average of d_{Co-Co} and d_{Co-Fe} (d_{Fe-Co} and d_{Fe-Fe}). In the random distribution of Fe, the probability to find Fe (Co) at the nearest-neighboring transition metal site is x $(1-x)$. Then, $d_{Co-M}(x)$ [$d_{Fe-M}(x)$] is expressed as $d_{Co-M}(x) = xd_{Co-Fe} + (1-x)d_{Co-Co}$ [$d_{Fe-M}(x) = xd_{Fe-Fe} + (1-x)d_{Fe-Co}$], where d_{Co-Co} (= 2.875(9) Å; Table 1), d_{Co-Fe} (= d_{Fe-Co}), and d_{Fe-Fe} are Co–Co, Co–Fe, and Fe–Fe distances, respectively. We use the crystallographic value (= 3.022 Å[18]) of NaFeO$_2$ for d_{Fe-Fe} while we used the extrapolated value (= 2.913 Å) of d_{Fe-M} at $x = 0$ for d_{Fe-Co} (see Fig. 4). The broken curves in Fig. 4 is the calculation of $d_{Co-M}(x)$ [$d_{Fe-M}(x)$]. Concerning to $d_{Co-M}(x)$, the calculation under random distribution satisfactory reproduces the experimental data. Concerning to $d_{Fe-M}(x)$, the calculation fails to reproduce the experimental data. The deviation between experiment and calculation indicates deviation from the random distribution of Fe. Here, we modify the probability to find M_g at the nearest-neighboring site as sx. $s = 1, > 1, < 1$ represent the random, attractive, and repulsive distribution, respectively (Fig. 1). Then, we obtained empirical equation as

$$d_{Fe-M}(x) = sxd_{Fe-Fe} + (1-sx)d_{Fe-Co}. \tag{1}$$

In general, an additional term such as constant*$x(1-x)$ is adopted to compensate the deviation between experimental data and the linear relation, because the term becomes zero at $x = 0$ and 1. We, however, applied a more straightforward expression (Eq. 1). The parameter (s) directly modifies the probability to find Fe at the nearest-neighboring site and has clear physical meaning. The red curve in Fig. 4 is the least-squares fitted results with Eq. (1). The fitted curve well reproduces the experimental data. The obtained s (= 4.8) is larger than unity, indicating that the Fe distribution has an aggregation tendency.

Discussion

The origin of the aggregation tendency of Fe is probably the distortion energy originated in the difference in the ionic radius between high-spin Fe^{3+} ($r = 0.645$ Å) than low-spin Co^{3+} ($r = 0.545$ Å). Actually, the lattice constant ($a = 3.022$ Å, $c = 16.074$ Å[18]) of NaFeO$_2$ is much larger than those ($a = 2.890$ Å, $c = 15.609$ Å[18]) of NaCoO$_2$. Then, the region where Fe and Co are mixed has extra distortion energy. Reflecting to this extra distortion energy, NaCo$_{1-x}$Fe$_x$O$_2$ has the phase-separation instability, or, spatially decomposition into $(1-x)$NaCoO$_2$ and xNaFeO$_2$. In the free energy point of view, the phase separation significantly decreases the entropy, and hence, is not realized

unless the gain of the internal energy is huge enough. Even if the phase separation is not realized, there remains the phase separation tendency, that is, the aggregation tendency of the guest Fe, as observed in Fig. 4.

In addition, we point out the Kinetics effect in synthesis. $NaCo_{1-x}Fe_xO_2$ were synthesized by sloid state reaction at relatively lower temperature (~ 850 K). In this situation, atomic migrations within the compound is not enough to reach the ground state. As a result, the compound remains in the metastable state with relatively random distribution. Amaha et al.[21] investigated chemical and structural inhomogeneity of two sets of $NaFe_{1/2}Co_{1/2}O_2$: one was prepared by quenching and the other was prepared by slowly-cooling after the synthesis at 1,173 K, respectively. They observed traces of inhomogeneity in the slowly-cooled compound while no trace of inhomogeneity was observed in the quenched one. This observation is consistent with the aggregation tendency of the guest Fe as detected the systematic EXAFS analyses against x in the present study.

Summary

We systematically investigated $d_{Co-M}(x)$ and $d_{Fe-M}(x)$ of $NaCo_{1-x}Fe_xO_2$ against x. We found that $d_{Fe-M}(x)$ steeply increases with increases in x. The x-dependence of $d_{Fe-M}(x)$ was analyzed by an empirical equation, $d_{Fe-M}(x) = sxd_{Fe-Fe} + (1-sx)d_{Fe-Co}$. The obtained s value (= 4.8) indicates the aggregation tendency of the guest Fe in $NaCo_{1-x}Fe_xO_2$. Thus, systematic EXAFS analysis against M_g concentration is a highly sensitive method to detect deviation from the random distribution of M_g in partially substituted materials.

Methods

Sample preparation and characterization. Layered oxides $NaCo_{1-x}Fe_xO_2$ were prepared by solid state reaction. Na_2O_2, Co_3O_4, and Fe_2O_3 were mixed in a 1.2:1–n:n atomic ratio and calcined at 858 K for 20 h in O_2. n (= 0, 0.002, 0.005, 0.010, 0.020, and 0.005) is the nominal Fe content. Then, the product was finely ground, and again calcined in the same condition. The actual Fe content (x) in $NaCo_{1-x}Fe_xO_2$ were determined by the inductively-coupled plasma (ICP) method as shown in Fig. S3 (x = 0, 0.002, 0.006, 0.012, 0.024, 0.060, respectively).

The X-ray diffraction (XRD) patterns were obtained using an X-ray powder diffractometer (MultiFlex, Rigaku, Tokyo, Japan) with the Bragg–Brentano (θ–2θ) geometry. The X-ray source was the Cu Kα line (λ = 1.5$\underline{4}$ Å) operated at 40 kV and 40 mA. The observed diffraction peaks can be indexed with O3-type structure ($R\underline{3}m$; Z = 3) without detectable impurities such as defect-spinel phases (Fig. S4). The lattice constants a and c were refined by the Rietveld analysis (Rietan-FP[22]) with a trigonal model ($R\underline{3}m$; Z = 3, hexagonal setting). Reflecting the larger ionic radius of Fe^{3+}, a and c increase with x (Fig. S5).

Local structural analysis by EXAFS. The extended X-ray absorption fine structure (EXAFS) measurements were conducted at BL-9A beamline of the Photon Factory, KEK. The synchrotron radiation was monochromatized by a Si (111) double-crystal monochromator. The energy resolution ($\Delta E/E$) was ~ 2×10^{-4} and the photon flux at sample position was ~ 4×10^{11} phs/s. The samples were finely ground, mixed with BN, and pressed into pellets with 5 mm in diameter. Co K-edge EXAFS spectra of $NaCo_{1-x}Fe_xO_2$ with x = 0.000, 0.002, 0.006, 0.012, 0.024, and 0.060 and Fe K-edge EXAFS spectra of $NaCo_{1-x}Fe_xO_2$ with x = 0.012, 0.024, and 0.060 were recorded in transmission mode with a gas-filled ion chamber at room temperature. Fe K-edge EXAFS spectra of $NaCo_{1-x}Fe_xO_2$ with x = 0.002, 0.006, and 0.012 were recorded in fluorescence mode using a 19-element solid-state detector (SSD). Before the SSD, a Mn filleter was used to remove the background signal from Co Kα fluorescence.

The background subtraction, normalization and analyses of EXAFS spectra were performed using the ATHENA program and EXAFS analyses were performed using the ARTEMIS programs[23] as described elsewhere[18,20]. First, the oscillatory components were extracted using the ATHENA program after background subtraction and normalization of the absorption spectra. Thus, we obtained $\chi(k)k^3 - k$ plots, where χ and k are the oscillatory components of the normalized absorption and angular wavenumber, respectively. Co and Fe K-edge EXAFS oscillations without any modelling results for $NaCo_{1-x}Fe_xO_2$ are shown in Figs. S6 and S7, respectively. The Fourier transformations of the $\chi(k)k^3$–R plots were performed in the k-range from 3.0 to 14.0 Å^{-1} at Co K-edge and from 2.0 to 8.5 Å^{-1} at Fe K-edge using the ATHENA program. In the plane wave and single-scattering approximation, $\chi(k)$ around the K-edge is expressed by the EXAFS equation as:

$$\chi(k) = -S_0^2 \sum_j \frac{N_j}{kR_j^2} F_j(k) e^{-2\sigma_j k^2} \sin\left\{2kR_j + \phi_j(k)\right\}, \tag{2}$$

where S_0, N_j, R_j, F_j, σ_j^2, and φ_j are the passive electron reduction factor, degeneracy of path, path length, effective scattering amplitude, mean square displacement, and effective scattering phase shift of the jth atom, respectively. The k is defined by $k = \sqrt{2m(E - E_o)/\hbar}$ where m, E, and E_0 are the electron mass, energy of the incident X-ray, and energy shift, respectively. In the least-squares curve fitting, we included the contribution from first (O), second (TM), and third (Na) nearest neighbor elements. We fixed N_j for the three elements at the crystallographic value ($N_1 = N_2 = N_3 = 6$). We used the same S_0 parameter for the three elements. The least-squares fittings were performed in q-space, which is inverse Fourier transformation in the R range from 1 to 3.22 Å. The best fitted results are shown in Figs. S8–S14.

Here, we consider the validity of the number of the free parameters (N_{fp}) in the EXAFS analysis. In general, N_{fp} should not exceed the maximum number of independent parameters ($N_{idp} = 2\Delta k\Delta R/\pi$)[24]. For Co K-edge EXAFS, N_{idp} is 15 since Δk is 11 Å^{-1} and ΔR is 2.22 Å. For Fe K-edge EXAFS, N_{idp} is 9 since Δk is 6.5 Å^{-1} and ΔR is 2.22 Å. Even if we exclude the k-range less than 3 which is not relevant to the EXAFS, N_{idp} for Fe K-edge EXAFS is 8. The free parameters used for analysis are S_0^2, E_0, d_{Fe-O}, d_{Fe-M}, d_{Fe-Na}, σ_{Fe-O}, σ_{Fe-M}, σ_{Fe-Na} for Fe K-edge EXAFS spectrum. Since S_0^2 is common for six spectra, the substantial N_{fp} is 7 + 1/6 for each Fe K-edge EXAFS spectrum.

Similarly, the free parameters used for analysis are S_0^2, E_0, d_{Co-O}, d_{Co-M}, d_{Co-Na}, σ_{Co-O}, σ_{Co-M}, σ_{Co-Na} for Co K-edge EXAFS spectrum. The substantial N_{fp} is $7 + 1/6$ for each Co K-edge EXAFS spectrum because S_0^2 is common for six Co spectra. Therefore. N_{fp} ($= 7 + 1/6$) is less than N_{idp} for both the Co and Fe K-edge EXAFS spectra.

Here, let us consider the difference between the error bar (σ_r) of interatomic distance (r) obtained by the EXAFS analysis and the experimental resolution (Δr) in Fourier transformed R-space. σ_r (e.g. 0.005–0.011 Å for d_{Fe-M}) is determined by the least-squares fitting of the experimental data by EXAFS Eq. (2). In general, the χ^2 statistic is defined as[25]

$$\chi^2 \equiv \sum_{i=1}^{n} \left\{ \frac{1}{\sigma_i^2} \left[y_i - y(x_i) \right]^2 \right\} \tag{3}$$

where y_i, $y(x_i)$, and σ_i are the observed values, calculated values, and uncertainty in y_i, respectively. In the present case, $y(x_i)$ are evaluated by the EXAFS Eq. (2) at x_i. Then, σ_r is given by.

$$\sigma_r = \sqrt{2 \left(\frac{\partial^2 \chi^2}{\partial r^2} \right)^{-1}}. \tag{4}$$

On the other hand, Δr is the lower limit value at which two peaks (shells) are separated and is given by $\Delta r = \pi/2\Delta k$, where $\Delta k = k_{max} - k_{min}$[26]. Δr for Fe (Co) K-edge EXAFS spectrum is 0.24 (0.14) Å. Thus, Δr is different from σ_r.

References

1. Yoshida, H., Yabuuchi, N. & Komaba, S. NaFe$_{0.5}$Co$_{0.5}$O$_2$ as high energy and power positive electrode for Na-ion batteries. *Electrochem. Commun.* **34**, 60–63 (2013).
2. Yabuuchi, N. *et al.* P2-type Na$_x$[Fe$_{1/2}$Mn$_{1/2}$]O$_2$ made from earth-abundant elements for rechargeable Na batteries. *Nat. Mater.* **11**, 512–517 (2012).
3. de Boisse, B. M., Carlier, D., Guignard, M. & Delmas, C. Structural and electrochemical characterizations of P2 and new O3-Na$_x$Mn$_{1-y}$Fe$_y$O$_2$ phases prepared by auto-combustion synthesis for Na–Ion batteries. *J. Electrochem. Soc.* **160**, A569–A574 (2013).
4. Mu, L. *et al.* Prototype sodium–ion batteries using an air-stable and Co/Ni-free O3-layered metal oxide cathode. *Adv. Mater.* **27**, 6928–6933 (2015).
5. Singh, G. *et al.* Electrochemical performance of NaFe$_x$(Ni$_{0.5}$Ti$_{0.5}$)$_{1-x}$O$_2$ (x = 0.2 and 0.4) cathode for sodium–ion battery. *J. Power Sources* **273**, 333–339 (2015).
6. Yue, J.-L. *et al.* O3-type layered transition metal oxide Na(NiCoFeTi)$_{1/4}$O$_2$ as a high rate and long cycle life cathode material for sodium ion batteries. *J. Mater. Chem. A* **3**, 23261–23267 (2015).
7. Takeda, H. *et al.* cu substitution effects on the local magnetic properties of Ba(Fe$_{1-x}$Cu$_x$)$_2$As$_2$: A site-selective ^{75}As and ^{63}Cu NMR study. *Phys. Rev. Lett.* **113**, 117001 (2014).
8. Machida, A., Moritomo, Y., Ohoyama, K., Katsufuji, T. & Nakamura, A. Phase separation and ferromagnetic transition in B-site substituted Na$_{1/2}$Ca$_{1/2}$MnO$_3$. *Phys. Rev. B* **65**, 064435 (2002).
9. Chen, X., Dong, S., Wang, K., Liu, J.-M. & Dagotto, E. Nonmagnetic B-site impurity-induced ferromagnetic tendency in CE-type manganese. *Phys. Rev. B* **79**, 024410 (2009).
10. Maikhuri, N., Panwar, A. K. & Jha, A. K. Investigation of A- and B-site Fe substituted BaTiO$_3$ ceramics. *J. Appl. Phys.* **113**, 3–6 (2013).
11. Delmas, C., Fouassier, C. & Hagenmuller, P. Structural classification and properties of the layered oxides. *Phys. B C* **99**, 81–85 (1980).
12. Yabuuchi, N., Yoshida, H. & Komaba, S. Crystal structures and electrode performance of alpha-NaFeO$_2$ for rechargeable sodium batteries. *Electrochemistry* **80**, 716–719 (2012).
13. Ichida, T., Shinjo, T., Bando, Y. & Takada, T. Magnetic properties of α-NaFeO$_2$. *J. Phys. Soc. Japan* **29**, 795–795 (1970).
14. McQueen, T. *et al.* Magnetic structure and properties of the S = 5/2 triangular antiferromagnet α-NaFeO$_2$. *Phys. Rev. B* **76**, 024420 (2007).
15. Lei, Y., Li, X., Liu, L. & Ceder, G. Synthesis and stoichiometry of different layered sodium cobalt oxides. *Chem. Mater.* **26**, 5288–5296 (2014).
16. Mikami, M. *et al.* Thermoelectric properties of two Na$_x$CoO$_2$ crystallographic phases. *Jpn. J. Appl. Phys.* **42**, 7383–7386 (2003).
17. Takada, K. *et al.* A new superconducting phase of sodium cobalt oxide. *Adv. Mater.* **16**, 1901–1905 (2004).
18. Akama, S. *et al.* Local structures around the substituted elements in mixed layered oxides. *Sci. Rep.* **7**, 43791 (2017).
19. Pfalzer, P. *et al.* Elimination of self-absorption in fluorescence hard-x-ray absorption spectra. *Phys. Rev. B.* **60**, 9335–9339 (1999).
20. Niwa, H., Kobayashi, W., Shibata, T., Nitani, H. & Moritomo, Y. Invariant nature of substituted element in metal-hexacyanoferrate. *Sci. Rep.* **7**, 13225 (2017).
21. Amaha, K., Kobayashi, W., Akama, S., Mitsuishi, K. & Moritomo, Y. Interrelation between inhomogeneity and cyclability in O3-NaFe$_{1/2}$Co$_{1/2}$O$_2$. *Phys. Status Solidi Rapid Res. Lett.* **11**, 1–6 (2017).
22. Izumi, F. & Momma, K. Three-dimensional visualization in powder diffraction. *J. Solid State Phemom.* **130**, 15–20 (2007).
23. Ravel, B. & Newwille, M. THENA, ARTEMIS, HEPHAESTUS: data analysis for X-ray absorption spectroscopy using IFEFFIT. *J. Synchrotron. Rad.* **12**, 537–541 (2005).
24. Penner-Hahn, J. E. X-ray absorption spectroscopy. In *Comprehensive Coordination Chemistry II* Vol. 2 (eds McCleverty, J. A. & Meyer, T. J.) 159–186 (Elsevier Ltd., New York, 2003).
25. Bevington, P. W. *Data Reduction and Error Analysis for the Physical Sciences* (McGraw-Hill, New York, 1969).
26. Walton, R. I. & Hibble, S. J. A combined in situ X-ray absorption spectroscopy and X-ray diffraction study of the thermal decomposition of ammonium tetrathiotungstate. *J. Mater. Chem.* **9**, 1347–1355 (1999).

Acknowledgements

Author contributions

T.M. performed sample preparations, characterizations, EXAFS measurements and analyses. H.N. provided advice on sample preparations, analyzed EXAFS, and wrote the manuscript. H.N. collaborated in EXAFS measurements at BL-9A of PF as a beamline staff. Y.M. planned the research and wrote the manuscript. All authors read and approved the manuscript.

Competing interests

Additional information

Supplementary information is available for this paper at https://doi.org/10.1038/s41598-020-68147-3.

Correspondence and requests for materials should be addressed to H.N. or Y.M.

Reprints and permissions information is available at www.nature.com/reprints.

Publisher's note Springer Nature remains neutral with regard to jurisdictional claims in published maps and institutional affiliations.